Isabel S. O. Barbosa[1,3]
João M. Costa[1,3]
Yaidelin A. Manrique[1,3]
Madalena M. Dias[1,3]
Joaquim L. Faria[1,3]
Ricardo J. Santos[1,3]
Cláudia G. Silva[1,3]
Margarida S. C. A. Brito[2,3,*]

ChannelCOMB Device for Mesostructured Reactors and Networks of Reactors

ChannelCOMB, a consecutive flow distributor, was constructed by additive manufacturing (AM) for experimental validation. The feasibility of using AM was experimentally analyzed for two techniques: stereolithography (tolerance of 50 µm) and fused deposition modeling (tolerance of 100 µm). For the best ChannelCOMB configuration, SLA printing shows a maximum of ca. 4 % in flow deviation, while FDM has a maximum of ca. 15 %. Thus, the SLA technique promotes better flow uniformity due to the fabrication tolerance and material permeability. The results also show that the experimental flow distribution measured for the best ChannelCOMB configuration printed by SLA can be well predicted by both computational fluid dynamics simulations and a model based on resistance analogs proposed in a previous work.

Keywords: Additive Manufacturing, ChannelCOMB devices, Flow distribution uniformity, Mesostructured reactors

Supporting Information available online

Received: November 18, 2022; *revised:* January 17, 2023; *accepted:* February 10, 2023

DOI: 10.1002/ceat.202200560

1 Introduction

Meso- and microchannel reactors have gained attention by the research community owing to their small size, leading to precise control of reaction variables due to high surface/volume ratio and the use of small quantities of reagents and solvent. These small-scale reactors have several applications in chemical engineering, biotechnology, the pharmaceutical industry, medicine, and environmental engineering [1]. They are also particularly used in the chemical industry for chemical synthesis [1], including organic synthesis [2], since they provide higher mass- and heat-transfer performance compared with conventional reactors. The scaleup from laboratory scale to pilot and industrial devices is typically carried out by numbering up the unit elements of a network of meso- and microchannels [3–5]. Generally, due to their dimensions, these devices operate in the laminar flow regime (low flow rates) [6].

Flow distribution uniformity is crucial for the successful performance of reactions in meso- and microchannel reactors operating as continuous flow systems [7–10]. The flow distribution ensures that all the channels operate under similar conditions of flow regime, mass transfer, and heat transfer [11–13]. The distribution of flow through several channels can be ensured by arrays of flow controllers or by manifold devices that split the flow through the channels. The main manifold device structures are known as consecutive and bifurcation. If the main fluid flow stream is split into several parallel streams, the distributor has consecutive configuration. In a bifurcation structure, the mainstream undergoes a standardized symmetric bifurcation, which enables doubling of the streams in a cascaded structure of several outlet flow channels. A detailed review of flow distributors has been presented by Barbosa et al. [7], in which a new consecutive flow distributor, namely ChannelCOMB, was introduced. Since then, more flow distributors have been studied and designed, and the most recent works are presented in Tab. 1.

The ChannelCOMB device consists of a single prismatic inlet channel in which the flow is divided for ten evenly spaced channels. Barbosa et al (2021) [7] studied the flow distribution using Computational Fluid Dynamics (CFD) simulations and a resistance analog model (RAM) developed by them [7]. ChannelCOMB is proposed as a device for construction by additive manufacturing (AM) [7]. Therefore, the best geometrical con-

[1]Isabel S. O. Barbosa, João M. Costa, Dr. Yaidelin A. Manrique, Prof. Madalena M. Dias, Dr. Joaquim L. Faria, Dr. Ricardo J. Santos https://orcid.org/0000-0002-9133-2187, Prof. Cláudia G. Silva
[1]Laboratory of Separation and Reaction Engineering–Laboratory of Catalysis and Materials (LSRE-LCM), Faculty of Engineering, University of Porto, Rua Dr. Roberto Frias, 4200-465 Porto, Portugal.
[2]Dr. Margarida S. C. A. Brito
https://orcid.org/0000-0003-1134-1743 (mbrito@fe.up.pt)
Laboratory for Process Engineering, Environment, Biotechnology and Energy (LEPABE), Faculty of Engineering, University of Porto, Rua Dr. Roberto Frias, 4200-465 Porto, Portugal.
[3]Isabel S. O. Barbosa, João M. Costa, Dr. Yaidelin A. Manrique, Prof. Madalena M. Dias, Dr. Joaquim L. Faria, Dr. Ricardo J. Santos https://orcid.org/0000-0002-9133-2187, Prof. Cláudia G. Silva, Dr. Margarida S. C. A. Brito https://orcid.org/0000-0003-1134-1743
[3]ALiCE Associate Laboratory in Chemical Engineering, Faculty of Engineering, University of Porto, Rua Dr. Roberto Frias, 4200-465 Porto, Portugal.

Table 1. Most recent flow distributors.

Distributor	Main results	Reference
ChannelCOMB device 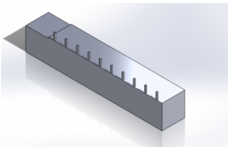	For Re[a] = 25 Maximum deviation of 1.4 %	[7]
Inlet contactors (T, Y, cross-T, and cross-Y) with splitting distributors 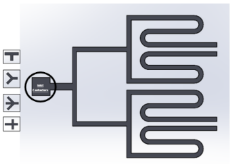	For $Q_{Water+SDS}$[b] > 5.32 mL min^{-1} Mean relative deviation of 14.65 %	[14]
Multistage pipe distributors 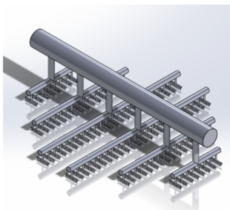	For average inlet velocity of v_{in} = 0.2 m s^{-1} Variance of $\sigma(v_{in})$ = 0.088	[15]
Ladder-tree distributor 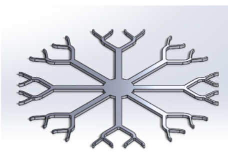	For $Q_{t,c}$[c] = 2 mL min^{-1} and $Q_{t,d}$[d] = 0.375 mL min^{-1} Coefficient of variation of < 0.05	[16]
Additively manufactured uniform fractal flow mixer 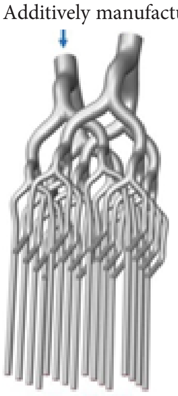	For Re_A = 100 and Re_B = 1000 Maximum relative standard deviation of ca. 8 %	[17]
Liquid distributor 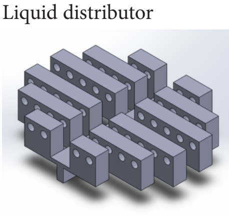	For spray densities of 5–120 m^{3}m^{-2}h^{-1} Maximum deviation of 5 %	[18]

[a] Reynolds number; [b] volumetric flow rate of water + sodium dodecyl sulfate; [c] theoretical flow rate of the continuous phase; [d] theoretical flow rate of the dispersed phase.

figuration and the tolerance of fabrication for three-dimensional (3D) printing were studied [7]. The results were analyzed on the basis of the maximum percentage deviation of flow rates between the ten channels. The best design showed a maximum deviation of 1.4 %.

Sain et al. [14] also studied a new configuration of flow distribution and showed the effect of inlet contactors (T, Y, cross-T, and cross-Y) of a microchannel distributor (see Tab. 1) on hydrodynamics parameters for gas-liquid flow uniformity. Based on the experimental results, a mean relative deviation of 14.65 % was found [14].

An et al. [15] developed CFD simulations and analytical models to determine fluid distribution in multistage pipe distributors on an industrial scale, as shown in Tab. 1. A double-convergence solution strategy was used to solve the analytical models based on empirical correlations of pressure recovery and discharge coefficients. The flow distribution was evaluated according to the variance, which was 0.088, leading to a uniform flow distribution [15].

Yi et al. proposed an improved ladder-tree distributor for use in scaleup production of monodisperse microspheres using microfluidic devices [16]. A sketch of the flow distributor is shown in Tab. 1.

Xue et al. [18] designed a narrow-trough liquid distributor with stepped baffle plates (see Tab. 1) to regulate liquid flow, which was studied by CFD simulation. The geometry led to uniform and stable flow of each distribution orifice [18].

Priyambodo et al. [17] used two different AM techniques (vat photopolymerization and laser powder bed fusion) to build a fractal flow mixer with bifurcating channels (see Tab. 1). CFD was used to simulate hydrodynamics and mixing in the distributor. The maximum relative standard deviation was ca. 8 %; thus, the flow was proved to be uniformly mixed [17].

Recently, fast prototyping tools have been intensively used for process design of flow distributions to overcome three issues: (1) the required modifications to the reactor design cannot be realized because of limitations of the available manufacturing technologies, (2) validation of the effectiveness of the changes can be too cost-intensive, and (3) fabrication would take too long [19]. Thus, the interest in AM as a technique to construct these reactors has increased, since in a few hours different reactor designs can be constructed and tested. All AM technologies follow the same principle, i.e., deposition of successive layers of materials to create 3D objects directly from a computer-generated model. AM has been employed in many applications, such as the design of (microfluidic) reactors [20–22], catalyst carriers and structured packings [23–25], tailored laboratory and reaction ware [26, 27], and flow distributors [17, 28].

AM reduces the gap between theory and experiments, enabling the construction of accurate device geometries optimized through CFD and the experimental evaluation of their performance [23]. Currently, the most widely used AM technologies are stereolithography (SLA), 3D-inject printing, selective laser sintering, and fused deposition modeling (FDM) [19]. This work focuses on SLA and FDM.

The first step of a 3D printing process is creating the 3D model. Then, the surface geometry of the 3D object and the slicing into digital layers are described in a an STL (standard tessellation language) file. Before transferring the model to the 3D printer, several parameters are defined, such as size, orientation of the AM layers, printing tolerance (layer depth), temperature, and fabrication materials [29, 30]. Materials such as curable resins in SLA or thermoplastic plastics in FDM are loaded and the printer is set up with printing parameters [30]. After manufacturing, the part is trimmed from the auxiliary structures and undergoes post-processing operations such as cleaning, polishing, and painting [30].

FDM is also known as fused filament fabrication (FFF) and it is a process of depositing thermoplastic filaments layer by layer on a build platform [31]. The first stage of FDM is the heating of the polymer filament to a semisolid state, which then is deposited on the print bed. The nozzle follows the path of the final object in the given layer and the material is extruded. This process occurs for every layer. The nozzle temperature, bed temperature, and layer height are the responsible parameters for the mechanical behavior of the 3D printed pieces [32].

SLA is a 3D printing technique based on photopolymerization reactions, i.e., a photocurable resin is solidified through photopolymerization initiated by absorbing light [33]. A photoinitiator is required to drive the polymerization reactions. The photopolymerization results in the solidification of a pattern inside the resin layer to hold the subsequent layers. The energy of the light source and exposure time are responsible for the thickness of the layer. The quality of SLA printed parts depends on fill cure depth, layer thickness, and post-curing. Usually, in SLA, the structures must be post-cured after printing to enhance their mechanical properties [34].

The main characteristics (operation mode, material type, printing scheme, advantages, and disadvantages) of FDM and SLA printing processes are described in Tab. 2.

AM is revolutionizing the manufacturing industry with the ability to produce accurately simple and highly complex geometries. Although the layer-by-layer construction remains the same, each technique has a distinctive process and different parameters of manufacturing. In order to understand the influence of FDM and SLA 3D printing processes for flow distribution uniformity in the ChannelCOMB device, several parameters, such as print materials, properties of printed parts, printing time, and layer resolution, are essential factors to be considered.

This work assesses the experimental validation of CFD simulations and the RAM for the best ChannelCOMB configuration proposed by Barbosa et al. [7]. They based the numerical design of ChannelCOMB on the dimensional tolerance in AM techniques. From the numerical work, an optimum design was reached. The numerical model of ChannelCOMB was used to analyze the flow rate distribution for different Reynolds numbers Re[1)] and geometric parameters: (1) expansion of chamber h, (2) outlet channels height h_{jets}, (3) outlet channels width w_{jets}, and (4) reactor depth e using CFD simulations and a RAM [7]. All the configurations studied and their flow distribution results are presented in Tab. 3.

Herein, the best geometries from the design study [7] were constructed by SLA and FDM. The results show that 3D print-

1) List of symbols at the end of the paper.

Table 2. Characteristics of FDM and SLA 3D printing processes.

	FDM	SLA
Operation	Material extrusion	UV curing
Material type	Solid (filament)	Liquid (resin)
Machine parameters [34]	Machine calibration	Laser power
	Nozzle diameter	Beam width
		Scan speed
Process parameters [34]	Raster angle	Fill cure depth
	Layer thickness	Layer thickness
	Extrusion width	Post-curing
	Feed rate/nozzle speed	
	Bed temperature	
	Nozzle temperature	
Printing scheme	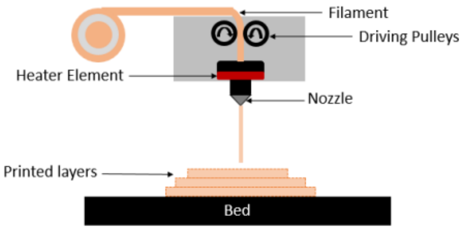	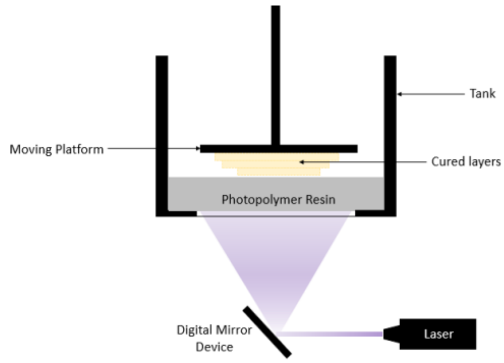
Advantages	Fast printing process	High-resolution parts
	Low part production cost	Wide range of functional applications
	Allows the use of a wide variety of materials	High accuracy and complexity
		Smooth surface areas
Disadvantages	Poor surface finish	Limited materials
	Support structures needed	High maintenance cost

ing is a powerful tool for the construction of flow distribution devices, enabling the development of competitive processes.

2 Methods and Materials

2.1 ChannelCOMB Device

Fig. 1 shows a sketch of ChannelCOMB and the parameters. The fluid is injected from a single inlet in a prismatic channel that has an expansion into a prismatic chamber, where the flow is distributed to an array of ten evenly spaced channels [7]. The geometric parameters of the three tested devices are listed in Tab. 4.

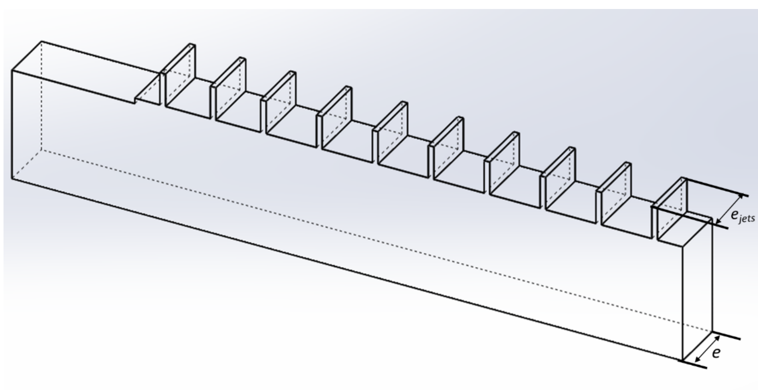

Figure 1. Sketch of ChannelCOMB.

Table 3. Geometric parameters for different ChannelCOMB configurations. Reprinted with permission from reference [7]. Copyright 2021 Elsevier.

Simulation	w_{jets} [mm]	h_{jets} [mm]	h [mm]	Re [–]	Max. deviation [%]
S0-Base	1.0	6.0	20	25	0.34
S1	1.0	6.0	20	100	1.60
S2	1.0	6.0	10	25	0.38
S3	1.0	6.0	1	25	0.04
S4	1.0	3.0	1	25	0.14
S5	1.0	1.0	1	25	3.60
S6	1.016	6.0	1	25	0.06
S7	1.036	6.0	1	25	0.07
S8	0.994	6.0	1	25	0.06
S9	1.0	6.0	20	33	0.48
S10	1.0	6.0	10	33	0.54
S11	1.0	6.0	1	33	0.09
S12	1.0	3.0	1	33	0.15
S13	1.0	1.0	1	33	3.15
S14	1.016	6.0	1	33	0.11
S15	1.036	6.0	1	33	0.10
S16	0.994	6.0	1	33	0.10

ChannelCOMB was analyzed according to its ability for uniform flow rate distribution by CFD and analytical models for different Reynolds numbers and several geometric parameters, namely ChannelCOMB10, ChannelCOMB20, and ChannelCOMBOptim in Barbosa et al. [7]. The ability of ChannelCOMB to uniformly distribute the inlet flow rate throughout the ten outlet channels was numerically demonstrated. 3D CFD simulations showed that the best design was obtained using ChannelCOMBOptim (see dimensions in Tab. 4) for an inlet velocity of $v_{in} = 0.00125\,m\,s^{-1}$ ($Re = 25$). Barbosa et al. (2021) [7] also simulated the influence of the SLA fabrication tolerance ($\pm$ 50 µm) on the outlet channel construction, and the results showed that the tolerance has an insignificant impact on the flow distribution, maximum deviations of flow rate in each channel below 8 % were obtained. Considering these results, it was concluded that AM technologies are suited for the construction of ChannelCOMB.

Table 4. ChannelCOMB dimensions.[a)]

	ChannelCOMB10	ChannelCOMB20	ChannelCOMBOptim
l [mm]	120	120	120
h_{in} [mm]	20	20	20
h_{jets} [mm]	6	6	6
h [mm]	1	1	1
w_{jets} [mm]	1	1	1
e [mm]	10	20	20
e_{jets} [mm]	10	20	1
s [mm]	10	10	10

[a)] l is the device length, h_{in} the inlet height, h_{jets} the outlet channel height, h the chamber expansion height, w_{jets} the outlet channel width, e the reactor depth, e_{jets} the outlet channels depth, and s the spacing between the outlet channels.

2.2 AM Techniques

FDM and SLA were applied in the construction of ChannelCOMB, and the differences between them in the uniformity of the flow distribution were assessed. Three ChannelCOMB configurations denoted ChannelCOMB10, ChannelCOMB20, and ChannelCOMBOptim were considered for this study, considering the CFD results and an RAM presented by Barbosa et al. [7]. The characteristics of the 3D printing processes are described in Tab. 5. All experiments were performed with water at $T \approx 20\,°C$.

Flow rate distribution and %deviation were assessed to study the performance of the device in flow distribution uniformity (Eq. (1)):

$$\%\text{Deviation} = \frac{|Q_i - \bar{Q}|}{\bar{Q}} \times 100 \tag{1}$$

where Q_i is the flow rate in channel i and $\bar{Q}$ the average flow rate.

Four inlet flow rates were tested experimentally and the respective Re value was calculated for each flow rate (Eq. (2)):

$$Re = \frac{\rho v_{in} d_h}{\mu} \tag{2}$$

where ρ is the fluid density, μ the fluid viscosity, and d_h the hydraulic diameter of the inlet (Eq. (3)):

$$d_h = \frac{(2e(h_{in} + h))}{((h_{in} + h) + e)} \tag{3}$$

The Re values were the same for ChannelCOMB20 and ChannelCOMBOptim, since the hydraulic diameters are also the same for these geometries.

Tab. 6. shows the flow rates measured at the prismatic inlet and the respective Re for each geometry.

3 Results and Discussion

The ChannelCOMB devices printed by SLA and FDM was tested for several Re numbers and their for flow distribution uniformity was assessed.

Table 5. Characteristics of FDM and SLA 3D printing processes for ChannelCOMB construction.

	FDM	SLA
3D Printer	BEETHEFIRST+ from Beeverycreative 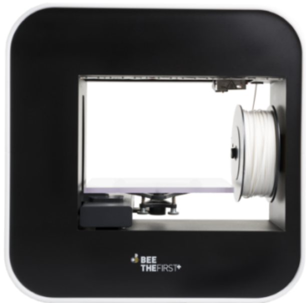	Form 2 from Formlabs 
Printing material	PLA filament	Clear V4 from Formlabs
Fabrication tolerance [µm]	100	50
ChannelCOMB10	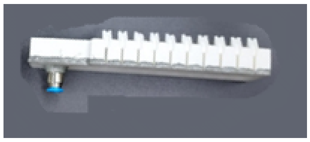	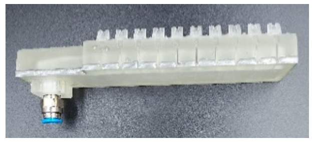
ChannelCOMB20	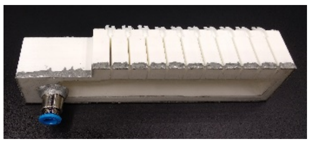	
ChannelCOMBOptim		

Table 6. Flow rate versus *Re*.

Geometry	Q [m^3s^{-1}]	Re [–]
ChannelCOMB10	1.18×10^{-6}	78
	1.77×10^{-6}	118
	2.36×10^{-6}	157
	2.95×10^{-6}	196
ChannelCOMB20 and ChannelCOMBOptim	1.18×10^{-6}	59
	1.77×10^{-6}	88
	2.36×10^{-6}	118
	2.95×10^{-6}	143

3.1 FDM Technique

The images of the tracer experiments with ChannelCOMB10, ChannelCOMB20, and ChannelCOMBOptim constructed by FDM are shown in the Supporting Information. The flow is randomly distributed through the outlet channel. Thus, a %deviation analysis was carried out to study which geometry ensures the most uniform flow distribution. Fig. 2 shows %deviation for FDM-ChannelCOMB10, FDM-ChannelCOMB20, and FDM-ChannelCOMBOptim for different working conditions.

Fig. 2 shows that both FDM-ChannelCOMB10 and FDM-ChannelCOMBOptim have a maximum deviation of flow rate at the outlet channels of 15 %, while FDM-ChannelCOMB20 has a maximum deviation of 19 %, leading to a poor flow distribution in this device. However, in the optimized geometry (FDM-ChannelCOMBOptim), the deviation is higher (≈ 15 %) only in the two first channels. Then for the remaining channels, the flow distribution is more uniform than in FDM-ChannelCOMB10, having a maximum deviation of approximately 10 %. Furthermore, according to Fig. 2, *Re* has no significant impact on flow distribution uniformity.

These results show that these geometries constructed by the FDM technique do not give the uniform flow distribution required for application in milli/meso multichannel reactors. These results can be explained by two facts: the tolerance of the FDM technique (100 µm) and the porosity of polylactic acid (PLA), which is the material used to print the geometry.

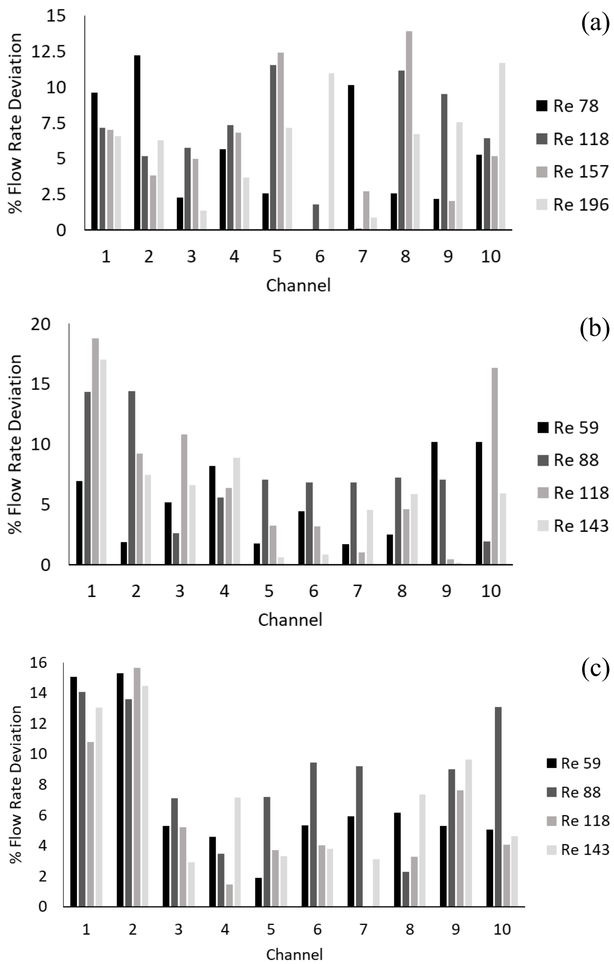

Figure 2. %Deviation of flow rate for (a) FDM-ChannelCOMB10, (b) FDM-ChannelCOMB20, and (c) FDM-ChannelCOMBOptim.

3.2 SLA Technique

The images of the tracer experiments with ChannelCOMB10, ChannelCOMB20, and ChannelCOMBOptim constructed by SLA are shown in the Supporting Information. For this technique, a random flow distribution through the outlet channel was also obtained. The deviation of flow rate at the outlet channels is shown in Fig. 3.

Fig. 3 shows that the optimized configuration (ChannelCOMBOptim) enables the best flow uniformity, because the maximum deviation is approximately 7 % for ChannelCOMBOptim but 10 and 14 % for ChannelCOMB10 and ChannelCOMB20, respectively. For SLA-printed devices, *Re* seems to have an impact on flow distribution, since increasing *Re* leads to less %deviation of the average flow rate, improving the flow distribution uniformity.

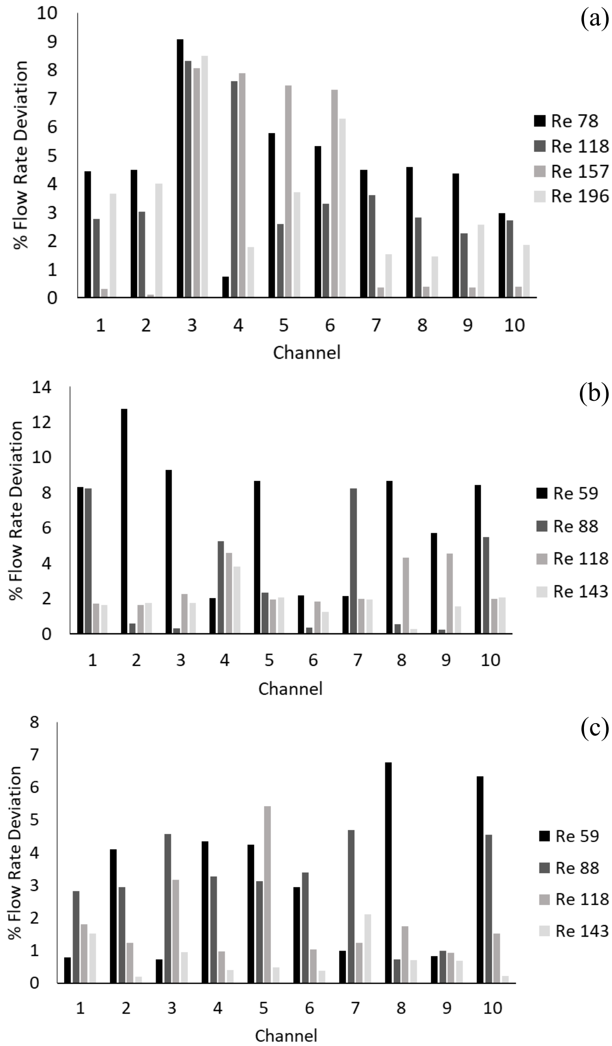

Figure 3. %Deviation of flow rate for (a) SLA-ChannelCOMB10, (b) SLA-ChannelCOMB20, and (c) SLA-ChannelCOMBOptim.

3.3 Comparison of AM Techniques

A comparison of SLA and FDM is shown in Fig. 4, which shows the maximum and average %deviation of the mean flow rate as a function of flow rate.

Comparing the SLA and FDM results in Fig. 4 reveals that the flow distribution uniformity seems to be influenced by the accuracy of the manufacturing technique. All the devices printed by SLA, which is the technique with lower tolerance (50 µm), show lower %deviation for all flow rates tested, that is, SLA promotes better flow distribution uniformity. Therefore, SLA has the capability of printing higher-resolution parts than FDM. Nevertheless, FDM is the most suitable technique in terms of printing simplicity, because the process basically consists of heating the polymer filament to a semisolid state and depositing it on the print bed. The SLA technique produced impermeable reactors. Reactors made by using FDM with PLA were slightly porous, which eventually led to leaking after long operation periods. Post-treatment with sealants, such as silicone, decreases this issue.

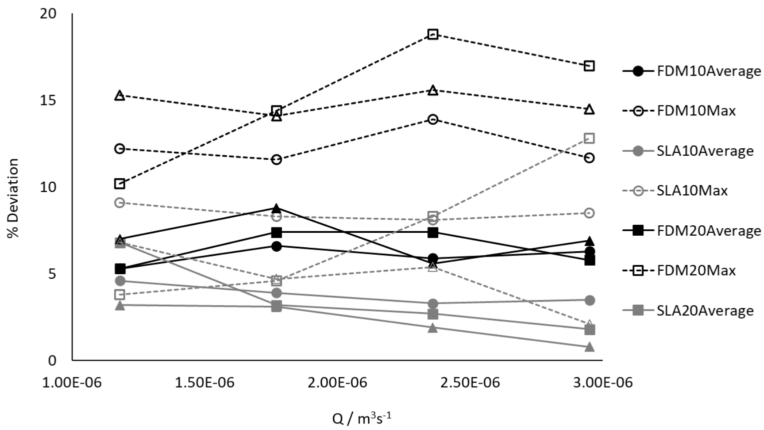

Figure 4. Maximum and average deviations of ChannelCOMB devices for SLA and FDM techniques.

3.4 Comparison of Experimental and Calculated Results

To validate the experimental results, a comparison between the experimental results, the RAM, and CFD results presented by Barbosa et al. [7] was made. Fig. 5a shows the flow distribution in ChannelCOMBOptim for experimental results for both techniques (SLA and FDM) at Re = 143, the RAM result determined by using the Excel solver at Re = 168, and the CFD result at Re = 168. Fig. 5b shows the %deviation of flow rate distribution for the same results. Note that the CFD simulations of Barbosa et al. [7] were performed for a random manufacturing tolerance that can not correspond to the real one (50 µm for SLA and 100 µm for FDM).

Fig. 5a shows that flow distributions determined from RAM and CFD simulations do not fit the flow distribution measured in experiments using the FDM technique, due to fabrication tolerance and the printing materials. This result shows, once again, that the 3D printing tolerance compromises the flow distribution in ChannelCOMBOptim.

On the other hand, the flow rate distributions determined by RAM and CFD simulations do not fit the experimental results obtained with the ChannelCOMBOptim printed by SLA, although they have the same order of magnitude. This result is expected, since the CFD simulations were not performed for the same manufacturing tolerance. However, Fig. 5b shows that the maximum deviation predicted by the model is ca. 5 %, that of the SLA experiments was ca. 4 %, and that of CFD was ca. 3 %, proving that there is a uniform flow distribution. These experimental results thus validate the CFD and RAM results presented by Barbosa et al. [7].

The energy consumption of the best configuration of ChannelCOMB was calculated, since the energy consumption in micro- and mesosized geometries is a major issue [35]. However, mesosized channels used to be more energy efficient than micro-sized channels. In this geometry, considering Re = 143, the dissipated power in the distributor is $P = Q\Delta p \approx 10^{-5}$ W for a flow rate of $Q = 2.36\times10^{-6}\,\mathrm{m^3s^{-1}}$. Thus, the pressure drop Δp in the system is not significant, resulting in low energy consumption.

4 Conclusion

This paper assesses the experimental validation of the flow distribution of ChannelCOMB, constructed by SLA and FDM AM techniques. Previous work studied the flow distribution in ChannelCOMB using CFD simulations and RAM. This work shows the influence of the two AM techniques and the validation of CFD and RAM models from experimental results.

For FDM, FDM-ChannelCOMBOptim is the best flow distributor configuration with a deviation of ca. 15 % when operated at Re = 143. The Reynolds number was found to have minimal impact on the flow distribution uniformity for this AM technique.

For SLA, SLA-ChannelCOMBOptim at Re = 143 showed a maximum deviation of ca. 4 %, corresponding to the geometry that promotes the best flow distribution uniformity. In the SLA case, increasing Reynolds number promotes better flow distribution.

In conclusion, the flow distribution uniformity is influenced by the manufacturing techniques and, therefore, it is recommended to resort to the SLA technique to construct a flow distribution applied to micro-/millireactors, which are very sensitive to differences in flow distribution. Furthermore,

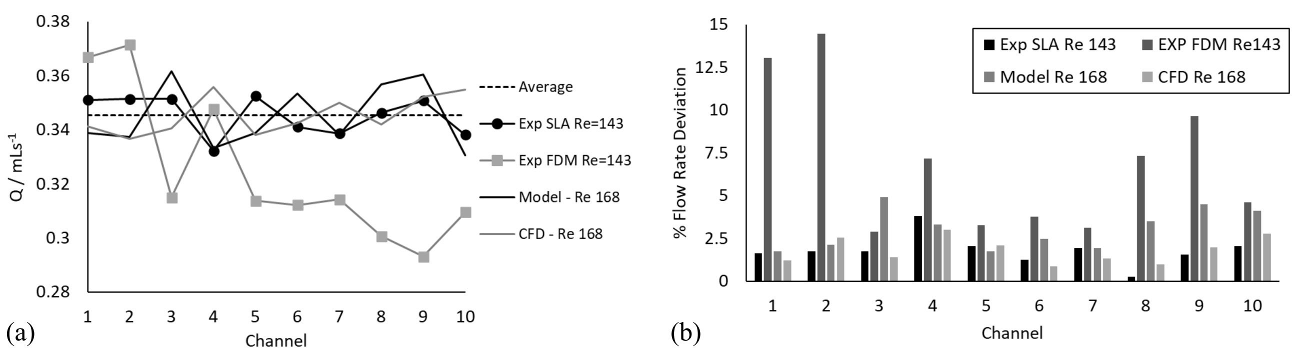

Figure 5. Experimental, CFD, and RAM results for ChannelCOMBOptim at Re = 143. (a) Flow distribution along the outlet channels and (b) %deviation comparison.

experimental results for the most accurate technique (SLA) validate the CFD simulations and RAM, showing that RAM can be implemented in future works to predict the flow distribution for other configurations.

Supporting Information

Supporting Information for this article can be found under DOI: https://doi.org/10.1002/ceat.202200560.

Acknowledgment

This work was financially supported by LA/P/0045/2020 (ALiCE), UIDB/50020/2020 and UIDP/50020/2020 (LSRE-LCM), and UIDB/00511/2020 and UIDP/00511/2020 (LEPABE) – funded by national funds through FCT/MCTES (PIDDAC). I. S. O. Barbosa acknowledges her FCT grant UI/BD/151092/2021.

The authors have declared no conflict of interest.

Symbols used

%deviation	[–]	percentage deviation of the mean flow rate
d_h	[m]	hydraulic diameter
e	[m]	reactor depth
e_{jets}	[m]	outlet channels depth
h	[m]	chamber expansion height
h_{in}	[m]	inlet height
h_{jets}	[m]	outlet channel height
l	[m]	device length
p	[Pa]	pressure drop
P	[W]	dissipated power
Q	[m^3s^{-1}]	volumetric flow rate
$\bar{Q}$	[m^3s^{-1}]	average volumetric flow rate
Q_i	[m^3s^{-1}]	volumetric flow rate in channel i
Re	[–]	Reynolds number
s	[m]	spacing between outlet channels
T	[°C]	temperature
v_{in}	[$m\,s^{-1}$]	inlet velocity
w_{jets}	[m]	outlet channel width

Greek letters

ρ	[$kg\,m^{-3}$]	fluid density
μ	[Pa s]	fluid viscosity

Abbreviations

AM	additive manufacturing
CFD	computational fluid dynamics
FDM	fused deposition modeling
FFF	Fused Filament Fabrication
PLA	polylactic acid
RAM	resistance analog model
SLA	stereolithography

References

[1] A. A. Bojang, H.-S. Wu, *Processes* **2020**, *8 (8)*, 891. DOI: https://doi.org/10.3390/pr8080891
[2] P. Watts, S. J. Haswell, *Chem. Eng. Technol.* **2005**, *28 (3)*, 290–301. DOI https://doi.org/10.1002/ceat.200407124
[3] M. F. Costa, C. M. Fonte, M. M. Dias, J. C. B. Lopes, *AIChE J.* **2017**, *63 (6)*, 2496–2508. DOI: https://doi.org/10.1002/aic.15473
[4] C. M. Fonte, M. E. Leblebici, M. M. Dias, J. C. B. Lopes, *Chem. Eng. Res. Des.* **2013**, *91 (11)*, 2250–2258. DOI: https://doi.org/10.1016/j.cherd.2013.07.014
[5] V. Hessel, H. Lowe, *Chem. Eng. Technol.* **2003**, *26 (5)*, 531–544. DOI: https://doi.org/10.1002/ceat.200390079
[6] J. M. Commenge, M. Saber, L. Falk, *Chem.Eng. J.* **2011**, *173 (2)*, 541–551. DOI: https://doi.org/10.1016/j.cej.2011.07.060
[7] I. S. O. Barbosa, R. J. Santos, C. G. Silva, M. S. C. A. Brito, *Chem. Eng. Process.* **2021**, *167*, 108541. DOI: https://doi.org/10.1016/j.cep.2021.108541
[8] N. S. Hanspal, A. N. Waghode, V. Nassehi, R. J. Wakeman, *Chem. Eng. J.* **2009**, *149 (1–3)*, 132–142. DOI: https://doi.org/10.1016/j.cej.2008.10.012
[9] R. L. Pigford, M. Ashraf, Y. D. Miron, *Ind. Eng. Chem. Fundam.* **1983**, *22 (4)*, 463–471. DOI: https://doi.org/10.1021/i100012a019
[10] P. H. Wang, W. T. Pan, G. C. Dai, *AIChE J.* **2020**, *66 (5)*, 16901. DOI: https://doi.org/10.1002/aic.16901
[11] M. Q. Pan, Y. Tang, L. Pan, L. S. Lu, *Chem. Eng. J.* **2008**, *137 (2)*, 339–346. DOI: https://doi.org/10.1016/j.cej.2007.05.012
[12] S. Park, I. Jung, Y. Lee, K. S. Kshetrimayum, J. Na, S. Park, S. Shin, D. Ha, Y. Lee, J. Chung, C.-J. Lee, C. Han, *Chem. Eng. Sci.* **2016**, *143*, 63–75. DOI: https://doi.org/10.1016/j.ces.2015.12.012
[13] E. V. Rebrov, J. C. Schouten, M. H. J. M. de Croon, *Chem. Eng. Sci.* **2011**, *66 (7)*, 1374–1393. DOI: https://doi.org/10.1016/j.ces.2010.05.044
[14] S. Sain, V. M. Rajesh, K. Gupta, S. Sinha Roy, *Ind. Eng. Chem. Res.* **2021**, *60 (46)*, 16682–16700. DOI: https://doi.org/10.1021/acs.iecr.1c02671
[15] M. An, X. Guan, N. Yang, *AIChE J.* **2021**, *68 (2)*, 17462. DOI: https://doi.org/10.1002/aic.17462
[16] H. Yi, S. Lu, J. Wu, Y. Wang, G. Luo, *Particuology* **2022**, *62*, 47–54. DOI: https://doi.org/10.1016/j.partic.2021.08.002
[17] M. D. M. Priyambodo, M. Mazur, J. Patel, M. Shah, B. Sun, V. Pareek, M. Brandt, P. A. Webley, T. Bhatelia, *Chem. Eng. Process.* **2022**, *179*, 109047. DOI: https://doi.org/10.1016/j.cep.2022.109047
[18] J. Xue, Q. Wu, H. Zhao, Q. Li, *AIChE J.* **2022**, *68 (10)*, 17806. DOI: https://doi.org/10.1002/aic.17806
[19] F. Guba, Ü. Tastan, K. Gugeler, M. Buntrock, T. Rommel, D. Ziegenbalg, *Chem. Ing. Tech.* **2018**, *91 (1–2)*, 17–29. DOI: https://doi.org/10.1002/cite.201800035
[20] B. S. Rupal, E. A. Garcia, C. Ayranci, A. J. Qureshi, *J. Integr. Des. Process Sci.* **2019**, *22 (1)*, 5–20. DOI: https://doi.org/10.3233/jid-2018-0001
[21] M. G. Gelhausen, T. Feuerbach, A. Schubert, D. W. Agar, *Chem. Eng. Technol.* **2018**, *41 (3)*, 618–627. DOI: https://doi.org/10.1002/ceat.201700294

[22] S. Waheed, J. M. Cabot, N. P. Macdonald, T. Lewis, R. M. Guijt, B. Paull, M. C. Breadmore, *Lab Chip* **2016**, *16 (11)*, 1993–2013. DOI: https://doi.org/10.1039/c6lc00284f

[23] C. Parra-Cabrera, C. Achille, S. Kuhn, R. Ameloot, *Chem. Soc. Rev.* **2018**, *47 (1)*, 209–230. DOI: https://doi.org/10.1039/c7cs00631d

[24] C. Busse, H. Freund, W. Schwieger, *Chem. Eng. Process.* **2018**, *124*, 199–214. DOI: https://doi.org/10.1016/j.cep.2018.01.023

[25] J. S. Manzano, Z. B. Weinstein, A. D. Sadow, I. I. Slowing, *ACS Catal.* **2017**, *7 (11)*, 7567–7577. DOI: https://doi.org/10.1021/acscatal.7b02111

[26] T. H. Lücking, F. Sambale, B. Schnaars, D. Bulnes-Abundis, S. Beutel, T. Scheper, *Eng. Life Sci.* **2015**, *15 (1)*, 57–64. DOI: https://doi.org/10.1002/elsc.201400094

[27] P. J. Kitson, M. D. Symes, V. Dragone, L. Cronin, *Chem. Sci.* **2013**, *4 (8)*, 3099–3103. DOI: https://doi.org/10.1039/c3sc51253c

[28] M. Mazur, T. Bhatelia, B. Kuan, J. Patel, P. A. Webley, M. Brandt, V. Pareek, R. Utikar, *Chem. Eng. Process.* **2019**, *143*, 107595. DOI: https://doi.org/10.1016/j.cep.2019.107595

[29] S. Rossi, A. Puglisi, M. Benaglia, *ChemCatChem* **2018**, *10 (7)*, 1512–1525. DOI: https://doi.org/10.1002/cctc.201701619

[30] I. Gibson, D. Rosen, B. Stucker, *Additive Manufacturing Technologies, 3D Printing, Rapid Prototyping and Direct Digital Manufacturing*, Springer, New York **2010**.

[31] A. D. Valino, J. R. C. Dizon, A. H. Espera, Q. Chen, J. Messman, R. C. Advincula, *Progr. Polym. Sci.* **2019**, *98*, 101162. DOI: https://doi.org/10.1016/j.progpolymsci.2019.101162

[32] J. Triyono, H. Sukanto, R. M. Saputra, D. F. Smaradhana, *Open Eng.* **2020**, *10 (1)*, 762–768. DOI: https://doi.org/10.1515/eng-2020-0083

[33] M. Pagac, J. Hajnys, Q. P. Ma, L. Jancar, J. Jansa, P. Stefek, J. Mesicek, *Polymers* **2021**, *13 (4)*, 598. DOI: https://doi.org/10.3390/polym13040598

[34] A. Kafle, E. Luis, R. Silwal, H. M. Pan, P. L. Shrestha, A. K. Bastola, *Polymers* **2021**, *13 (18)*, 3101. DOI: https://doi.org/10.3390/polym13183101

[35] S. Arockiam, Y. H. Cheng, P. M. Armenante, S. Basuray, *Chem. Eng. Res. Des.* **2021**, *167*, 303–317. DOI: https://doi.org/10.1016/j.cherd.2021.01.022

